HyperFree: A Channel-adaptive and Tuning-free Foundation Model for Hyperspectral Remote Sensing Imagery

Supplementary Material

1. Hyper-Seg Data Engine

1.1. Wavelength Selection

To utilize the spectral information rather than only the RGB channels, Hyper-Seg engine separates the original image into 3 groups with different wavelength combination, where we refer to the famous Landsat-8 satellite in Table 1. The selected wavelengths represents the valuable practical experience and cover the overall range from $0.4 \sim 2.5\,\mu$m.

Table 1. Statistical results of classical multispectral satellites about the selected wavelengths, supporting the wavelength selection of Hyper-Seg data engine and the weight dictionary $\boldsymbol{\beta_k}$.

Satellite	Central Wavelengths(nm)
Landsat-7	482.5, 565, 660, 825, 2220, 1650, 11450
Landsat-8	443, 482.5, 562.5, 655, 865, 1610, 1375, 2200, 10895, 12005
Sentinel-2A/2B	443, 490, 560, 665, 705, 740, 783, 842, 865, 945, 1375, 1610, 2190
WorldView-2/3	425, 480, 545, 605, 660, 725, 832.5, 950
ZY1-02D/E	486.5, 564.5, 662.5, 835.5, 434, 612, 730, 959
ZY-3	485, 555, 660, 830
RapidEye	455, 555, 655, 710, 805
PlanetScope	485, 545, 630, 820
GeoEye-1	480, 545, 672.5, 850
SPOT-6/7	485, 560, 655, 825
Pleiades-1A/B	490, 560, 650, 840
IRS-P6	555, 640, 815, 1625
KOMPSAT-2/3/4	485, 560, 660, 830
GF-1/2	485, 555, 660, 830
GF-4	485, 560, 660, 830, 3800
GF-6	485, 555, 660, 830, 720, 750, 425, 610

1.2. Statistical Information

Figure 1 reports the statistical information of constructed Hyper-Seg dataset. With the non-maximum suppression (NMS) operation, the number of final combined masks is approximately 2 to 3 times the number of masks for each group separately as in Figure 1 (a), indicating that Spectral-Seg can utilize the spectral information effectively. From Figure 1 (b) and Figure 1 (c), it can be observed that the number density of generated masks in the three source datasets is roughly equivalent and the small masks dominate the dataset, increasing the segmentation difficulty.

2. Selection of Key Channels in Weight Dictionary

In proposed channel-adaptive embedding layer, we design a sperate branch for processing key channels, which are set according to the successful prior of launched satellites in Table 1. Each wavelength in Table 1 is selected by expert knowledge. To merge the wavelengths that almost overlap between different satellites, we sort all the wavelengths first, take the average of every two adjacent wavelengths with interval less than 10nm (common spectral resolution) and substitute them. Combining with the longest wavelength 2500nm, a total of 85 wavelengths were selected to build the learnable dictionary $\boldsymbol{\beta_k}$.

3. Overview of Experimental Datasets

All the used public datasets are summarized in Table 2, which have different channel numbers and spectral ranges. We have tested both the tuning-free manner and tunning manner in five tasks including HC, HOCC, HTD, HAD and HCD. Due to the different output formats, only tuning manner is applied on HD, HU and HOT tasks.

Table 2. Summary of used public datasets on the eight tasks.

Tasks	Datasets	Number of Channels	Spectral Range (nm)
HC	LongKou [55]	270	$400 \sim 1000$
	HanChuan [55]	274	$400 \sim 1000$
	HongHu [55]	270	$400 \sim 1000$
HOCC	HongHu [55]	270	$400 \sim 1000$
	XiongAn [50]	256	$390 \sim 1000$
HTD	Airport [2]	205	$400 \sim 2500$
	Cri [51]	46	$650 \sim 1100$
HAD	Beach-1 [2]	188	$430 \sim 860$
	Beach-2 [2]	193	$430 \sim 860$
HCD	Hermiston [12]	154	\
	River [12]	198	$400 \sim 2500$
HD	Washington D.C. [3]	191	$400 \sim 2400$
HU	Urban [15]	162	$400 \sim 2500$
HOT	HOTC 2023 [1]	56	$460 \sim 960$

4. Additional Experiments

4.1. Qualitative Results in Tuning-free Manner

Complete visualization results are shown for five tasks. (a) Figure 3, 4 and 5 for HC task. (b) Figure 6 and 7 for HOCC task . (c) Figure 9 and 8 for HTD task. (d) Figure 10 and 11 for HAD task. (e) Figure 12 and 13 for HCD task. With the powerful segmentation ability and PMF interaction, HyperFree can achieve the best visualization performance without

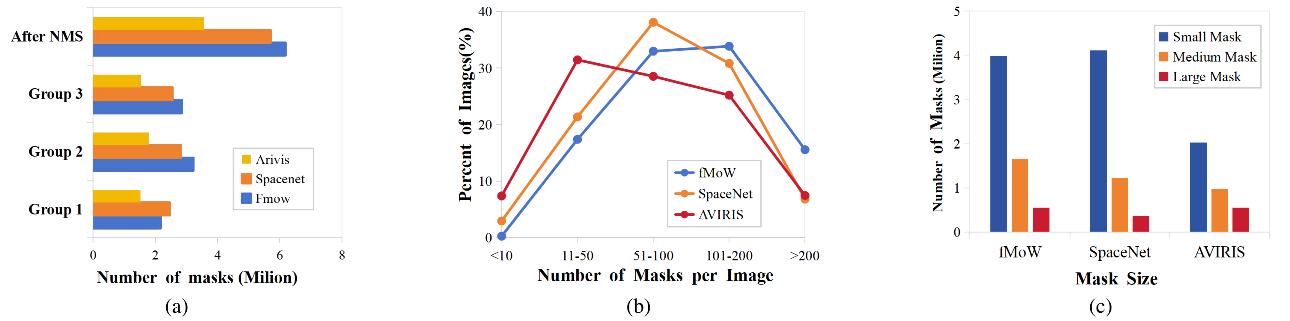

Figure 1. Some statistical information about the built large-scale Hyper-Seg dataset.

tuning compared to the specialized models training with 5 shots.

4.2. Quantitative and Qualitative Results With Tuning

We have also tested the further tuning performance of HyperFree as an extensive experiment. The tuned version is denoted as HyperFree* for simplicity. The quantitative results are reported in Table 4 ∼ Table 11 for HC, HOCC, HTD, HAD, HCD, HD, HU and HOT tasks, respectively. For the five tasks supporting the tuning-free manner, the qualitative results of HyperFree* are put together with results in Section 4.1. The qualitative results of HD, HU and HOT tasks are shown in Figure 14, 15 and 16, respectively. After tuning, HyperFree has achieved the best performance in most datasets and tasks. Since HyperFree is proposed mainly for tuning-free manner, we use the full-tuning setting directly without using any advanced tuning methods.

Table 3. Execution time comparison with deep models on five tuning-free tasks.

HC	SSFTT [41]	MambaHSI [22]	HyperFree
	197.08s	429.86s	7.85s(1st)
HOCC	OC Loss [53]	T-HOneCls [52]	HyperFree
	244.46s	344.48s	21.50s(1st)
HTD	HTD-IRN [40]	TSTTD [14]	HyperFree
	25.05s	378.40s	9.85s(1st)
HAD	Auto-AD [43]	TDD [18]	HyperFree
	78.81s	28.31s	11.72s(1st)
HCD	BIT [5]	SST-Former [45]	HyperFree
	142.23s	116.05s	15.90s(1st)

4.3. Sensitivity Analysis

Prompt Number. In the five tuning-free tasks, HC and HOCC need prompts of each category to generate the semantic-aware results. We explored the relationship between model performance and the number of prompts as in Figure 2. The mean and std of metrics are calculated for each prompt number with 10 repeat experiments. We found HyperFree is mostly insensitive to the prompt number in

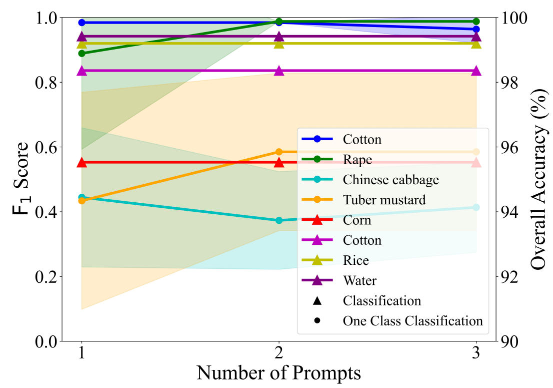

Figure 2. Sensitivity analysis of the prompt number on the model performance (HC and HOCC tasks).

both tasks and one prompt is good enough.

Hyperparameter τ. HyperFree completes five tasks directly with the PMF interaction, where the two interaction modes are used adaptively with the hyperparameter τ. To explore its sensitivity, we have varied it and reported the corresponding results in Figure 17. HC task is not included since it does not need any τ. Most tasks show a certain but acceptable sensitivity to τ, where the HTD and HCD tasks exhibit more variation. Despite this, the fluctuation range of the metrics remains within an acceptable range of 0.1.

4.4. Execution Efficiency Comparison Experiments

Without the tuning process, HyperFree can reduce the processing time by $1 \sim 2$ orders of magnitude compared to other deep models as in Table 3.

Table 4. Quantitative comparison results on HC task in tuning manner, where HyperFree* represents the tuning version and blue numbers indicate the metric ranking.

Dataset	Metric	SVM [28] (5 shot)	HybridSN [38] (5 shot)	FullyContNet [42] (5 shot)	FPGA [54] (5 shot)	SSFTT [41] (5 shot)	MambaHSI [22] (5 shot)	HyperFree* (5 shot)
LongKou [55]	OA	82.77	48.78	86.67	91.18	89.66	92.65	92.10(2nd)
	AA	74.02	61.37	85.6	88.35	87.96	92.57	92.71(1st)
	KA	78.04	35.72	82.3	88.66	87.95	90.00	89.85(2nd)
HanChuan [55]	OA	52.68	47.75	55.55	71.47	64.86	73.33	83.56(1st)
	AA	47.76	46.17	59.72	72.09	61.22	69.33	82.21(1st)
	KA	46.85	41.31	50.18	67.58	59.65	69.1	81.03(1st)
HongHu [55]	OA	52.89	31.22	55.84	80.55	64.31	78.96	81.65(1st)
	AA	45.97	34.14	67.25	75.12	64.53	76.02	85.56(1st)
	KA	45.47	24.51	49.67	75.74	57.79	73.29	77.58(1st)

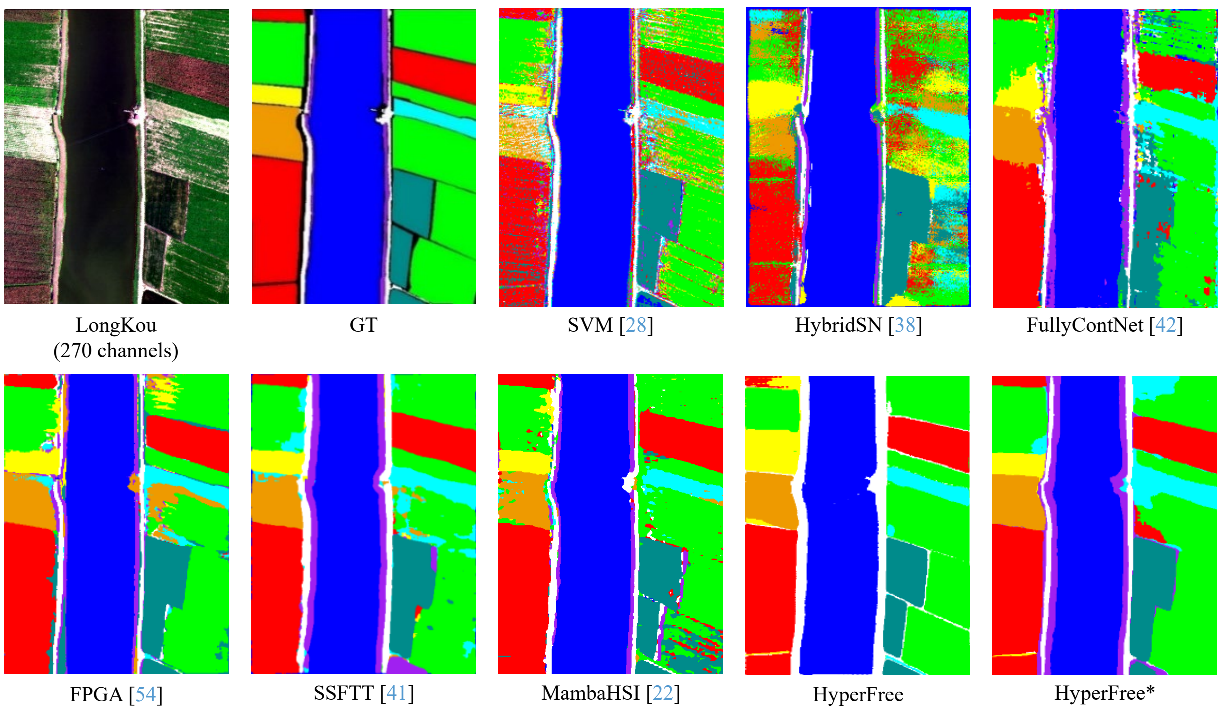

Figure 3. Qualitative comparison results on LongKou dataset of HC task, where HyperFree* represents the tuning version.

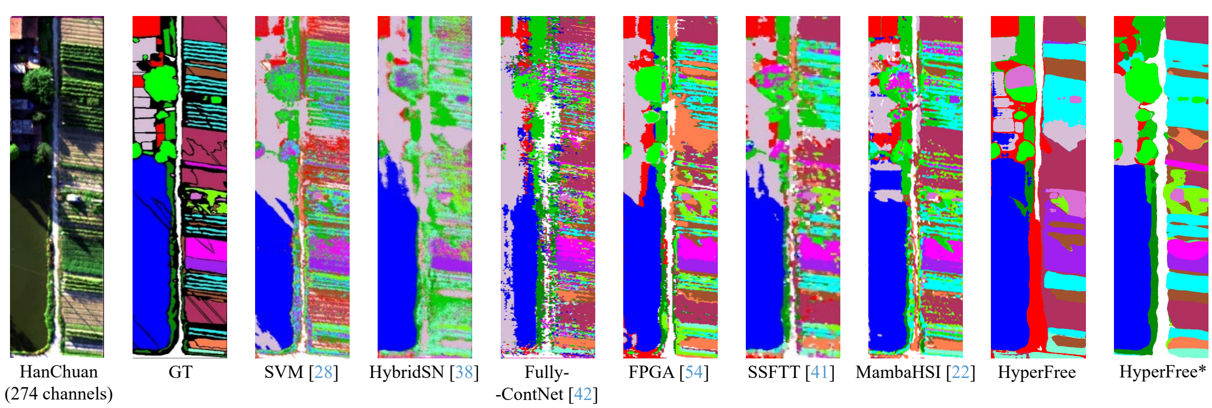

Figure 4. Qualitative comparison results on HanChuan dataset of HC task, where HyperFree* represents the tuning version.

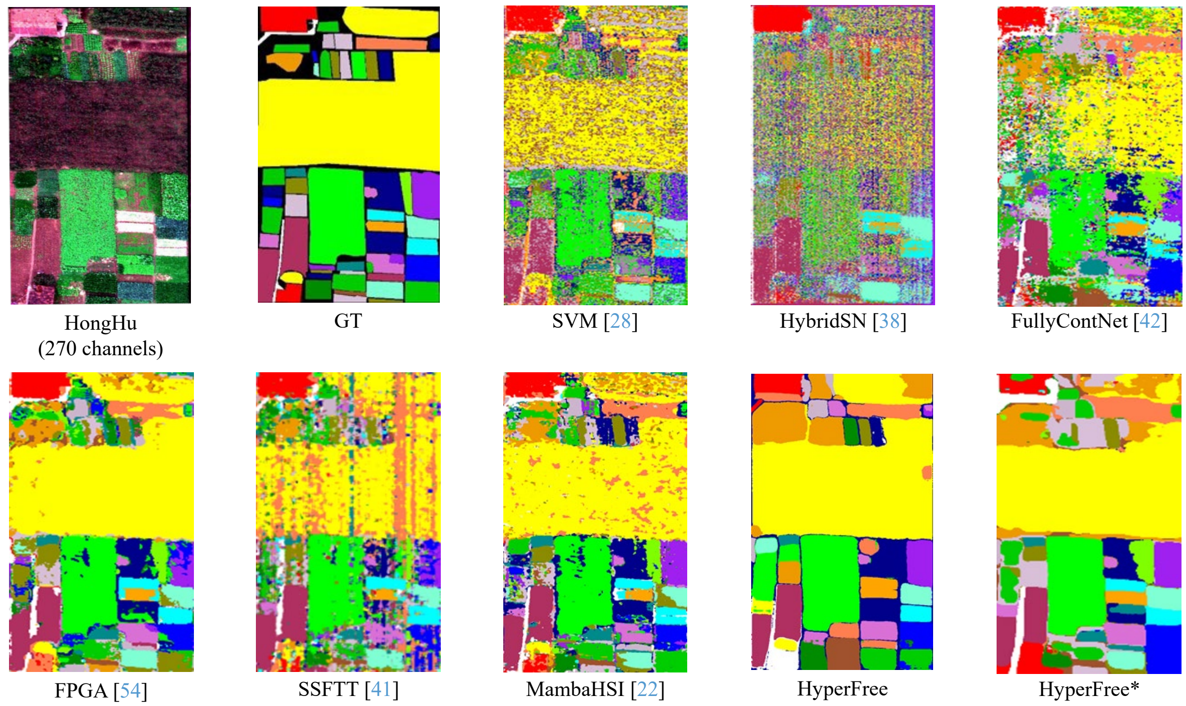

Figure 5. Qualitative comparison results on HongHu dataset of HC task, where HyperFree* represents the tuning version.

Table 5. Quantitative comparison results on HOCC task in tuning manner, where HyperFree* represents the tuning version and blue numbers indicate the metric ranking.

Dataset	Metric	OCSVM [39] (5 shot)	nnPU [16] (5 shot)	BSVM [33] (5 shot)	PAN [13] (5 shot)	OC Loss [53] (5 shot)	T-HOneCls [52] (5 shot)	HyperFree* (5 shot)
HongHu [55]	F_1	26.33	19.13	34.82	63.69	54.73	72.52	91.24(1st)
	P	56.43	19.72	50.79	75.00	58.26	46.52	92.77(1st)
	R	24.02	18.58	45.29	64.27	54.34	92.35	89.90(2nd)
XiongAn [50]	F_1	18.31	1.76	26.30	46.34	43.08	41.34	66.89(1st)
	P	39.83	2.85	23.82	47.13	47.50	32.87	61.94(1st)
	R	16.08	1.98	57.83	53.32	47.61	60.38	75.74(1st)

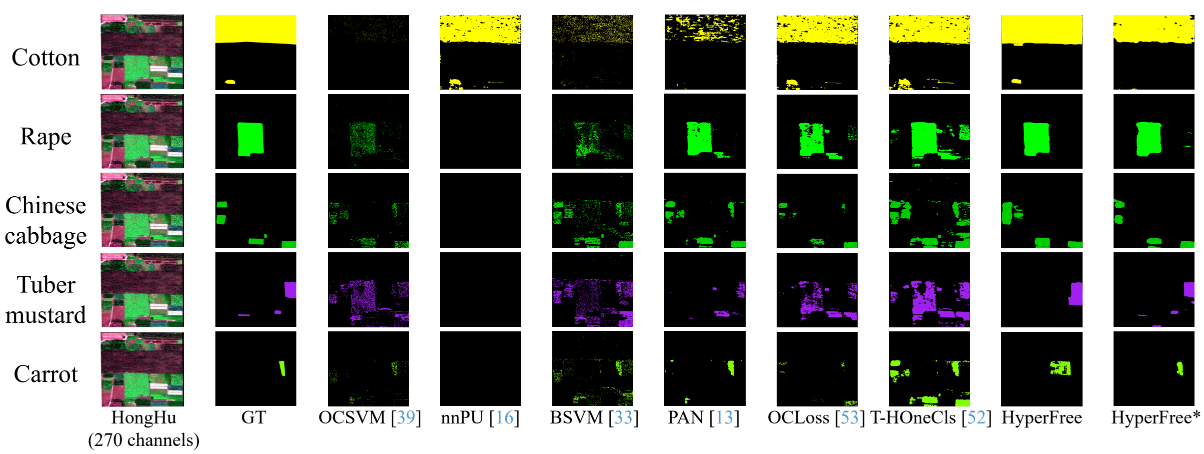

Figure 6. Qualitative comparison results on HongHu dataset of HOCC task, where HyperFree* represents the tuning version.

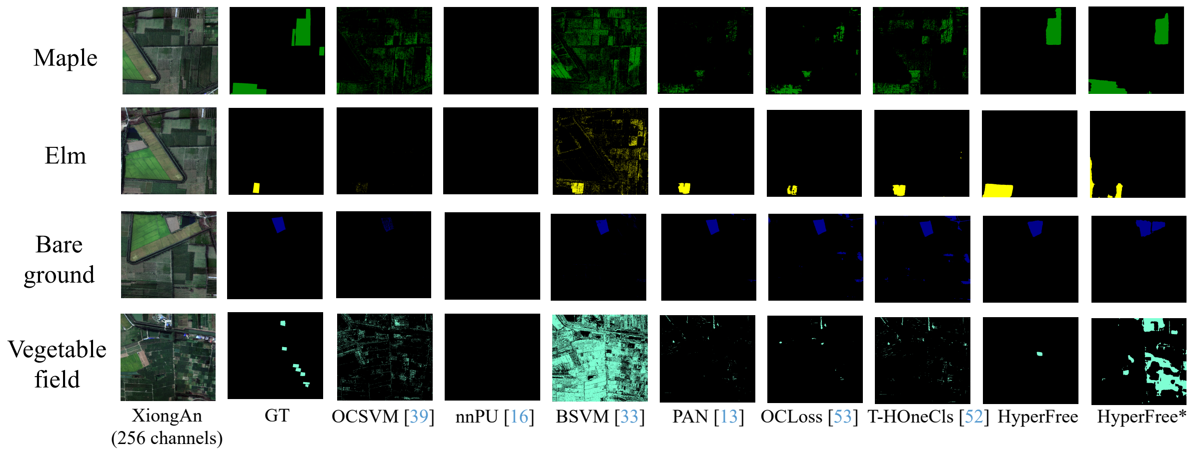

Figure 7. Qualitative comparison results on XiongAn dataset of HOCC task, where HyperFree* represents the tuning version.

Table 6. Quantitative comparison results on HTD task in tuning manner, where HyperFree* represents the tuning version and blue numbers indicate the metric ranking.

Dataset	Metric	ACE [17] (1 shot)	CEM [4] (1 shot)	GLRT [26] (1 shot)	MF [27] (1 shot)	HTD-IRN [40] (1 shot)	TSTTD [14] (1 shot)	HyperFree* (1 shot)
Airport [2]	$AUC_{(D,F)}$	0.9794	0.9603	0.9801	0.9916	0.9745	0.9929	0.9937(1st)
	AUC_{ODP}	1.5853	1.2829	1.5798	1.6968	1.4484	1.6592	1.5945(3rd)
Cri [51]	$AUC_{(D,F)}$	0.9735	0.9893	0.9737	0.9891	0.9975	0.9987	0.9976(2nd)
	AUC_{ODP}	1.2015	1.4506	1.2	1.4575	1.3995	1.6103	1.4821(2nd)

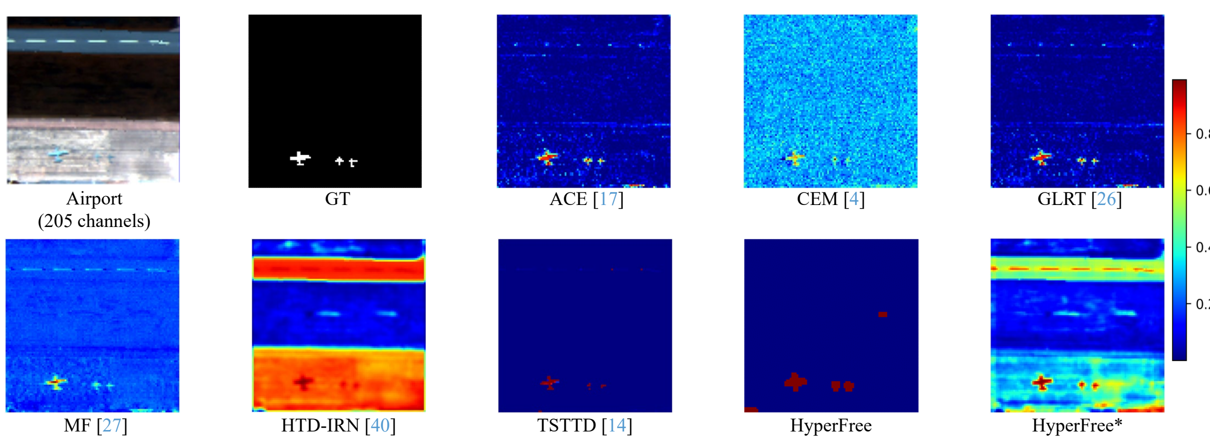

Figure 8. Qualitative comparison results on Airport-4 dataset of HTD task, where HyperFree* represents the tuning version.

Table 7. Quantitative comparison results on HAD task in tuning manner, where HyperFree* represents the tuning version and blue numbers indicate the metric ranking.

Dataset	Metric	RXD [37]	CRD[20]	ADLR [36]	LRASR [49]	Auto-AD [43]	TDD [18]	HyperFree*
Beach-1 [2]	$AUC_{(D,F)}$	0.9815	0.9471	0.4515	0.7461	0.9574	0.9842	0.9973(1st)
	AUC_{ODP}	1.2557	0.9785	0.561	0.8526	1.1273	1.1383	1.7862(1st)
Beach-2 [2]	$AUC_{(D,F)}$	0.909	0.8544	0.7976	0.8225	0.9485	0.9627	0.9715(1st)
	AUC_{ODP}	1.0177	0.867	0.9064	0.828	1.0097	1.1688	1.3900(1st)

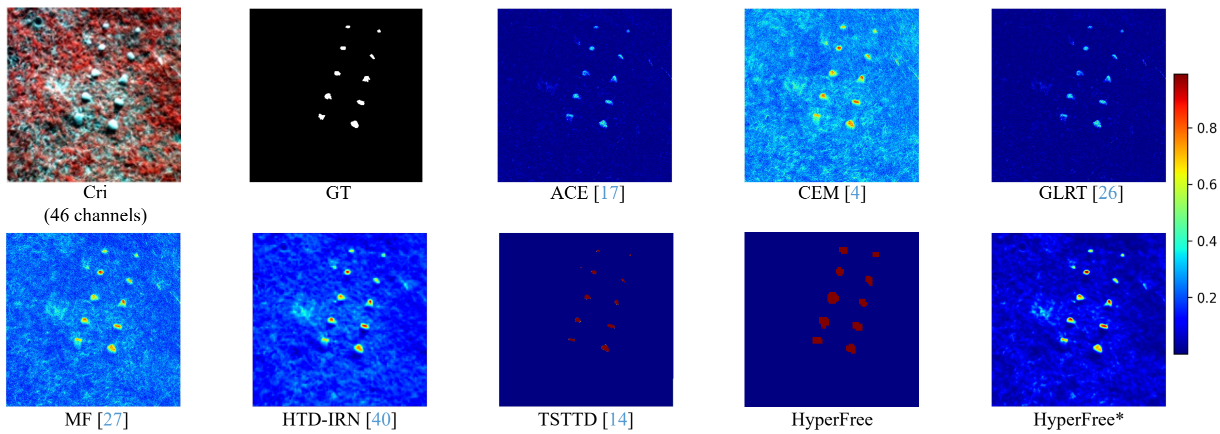

Figure 9. Qualitative comparison results on Cri dataset of HTD task, where HyperFree* represents the tuning version.

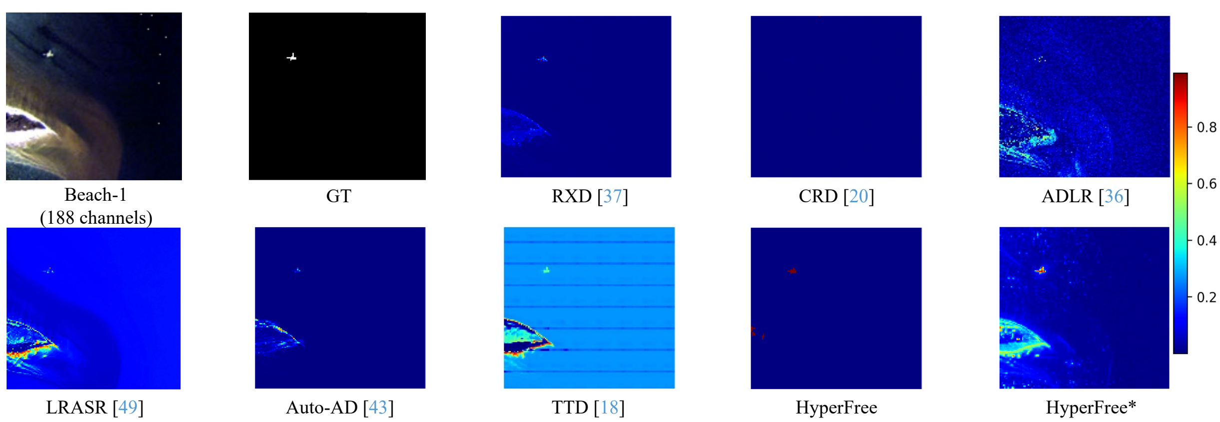

Figure 10. Qualitative comparison results on Beach-1 dataset of HAD task, where HyperFree* represents the tuning version.

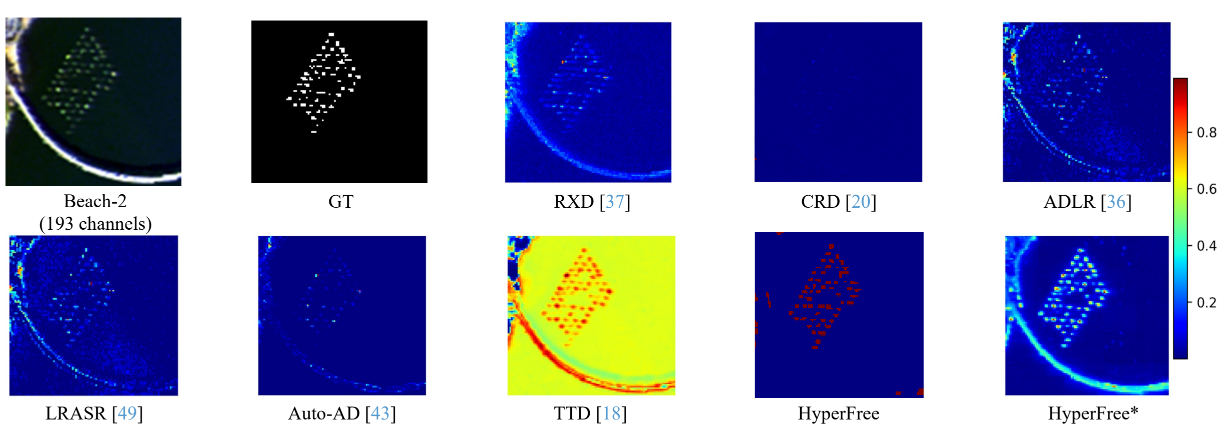

Figure 11. Qualitative comparison results on Beach-2 dataset of HAD task, where HyperFree* represents the tuning version.

Table 8. Quantitative comparison results on HCD task in tuning manner, where HyperFree* represents the tuning version and blue numbers indicate the metric ranking.

Dataset	Metric	FC-EF [7] (5 shot)	FC-Sc [7] (5 shot)	FC-Sd [7] (5 shot)	ML-EDAN [34] (5 shot)	BIT [5] (5 shot)	SST-Former [45] (5 shot)	HyperFree* (5 shot)
Hermiston [12]	IoU	37.29	37.76	48.73	32.52	52.57	53.61	61.58(1st)
	F_1	54.32	54.82	65.52	49.08	68.91	69.8	76.22(1st)
River [12]	IoU	41.68	45.22	45.34	39.15	21.26	40.96	47.16(1st)
	F_1	58.84	62.28	62.39	56.28	35.07	58.12	64.09(1st)

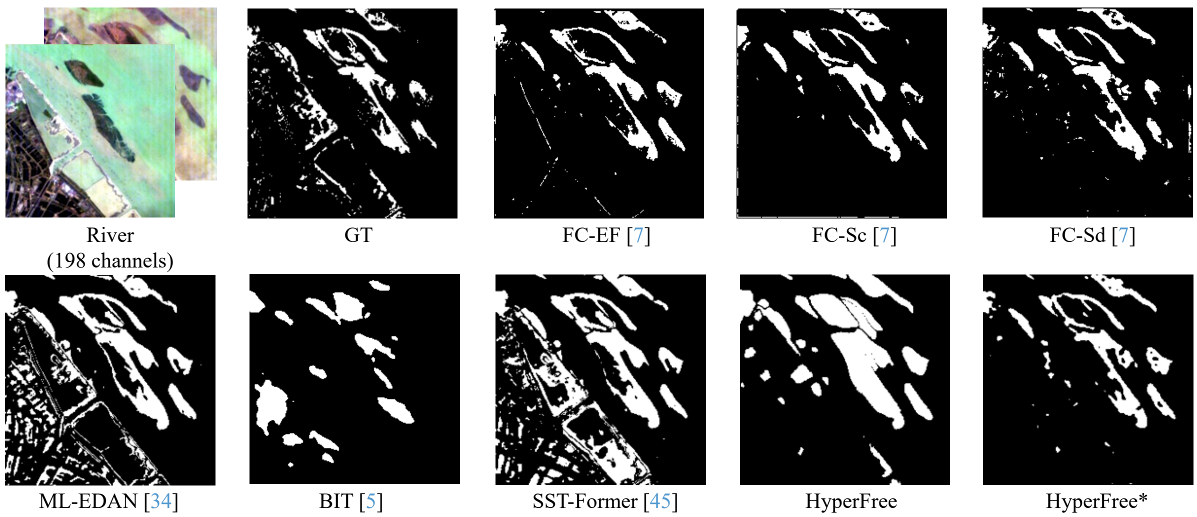

Figure 12. Qualitative comparison results on River dataset of HCD task, where HyperFree* represents the tuning version.

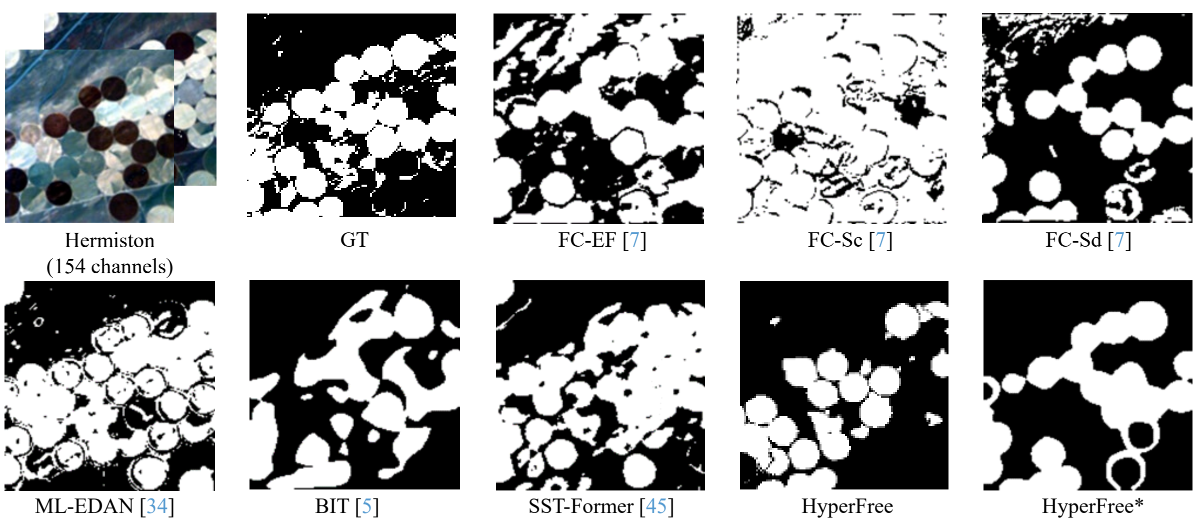

Figure 13. Qualitative comparison results on Hermiston dataset of HCD task, where HyperFree* represents the tuning version.

Table 9. Quantitative comparison results on HD task in tuning manner, where HyperFree* represents the tuning version and blue numbers indicate the metric ranking.

Dataset	Metrics	NGMee [9]	LRTFL$_0$ [47]	E-3DTV [32]	QRNN3D [46]	DS2DP[29]	SST [19]	HyperFree*
Washington D.C. [3]	PSNR	23.89	25.58	25.97	27.79	27.31	28.1	28.49(1st)
	SSIM	0.872	0.907	0.921	0.945	0.937	0.989	0.990(1st)
	SAM(°)	14.89	11.35	8.772	7.563	7.735	6.343	6.251(1st)

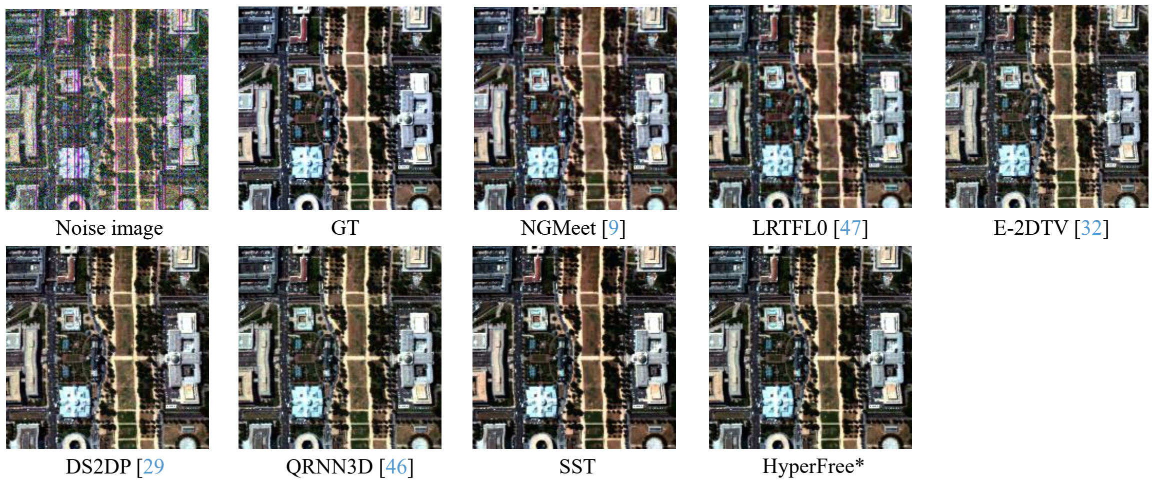

Figure 14. Qualitative comparison results on Washington D.C. dataset of HD task, where HyperFree* represents the tuning version.

Table 10. Quantitative comparison results on HU task in tuning manner, where HyperFree* represents the tuning version and blue numbers indicate the metric ranking.

Dataset	Metric	VCA-FCLS [10, 30]	SGSNMF [44]	uDAS [35]	CNNAEU [31]	CyCU-Net [8]	GSUU [6]	HyperFree*
Urban [15]	SAD	0.3859	0.4442	0.6498	0.5364	0.2750	0.1645	0.0446(1st)
	RMSE	0.1061	0.0973	0.1009	0.0392	0.1597	0.1188	0.0170(1st)

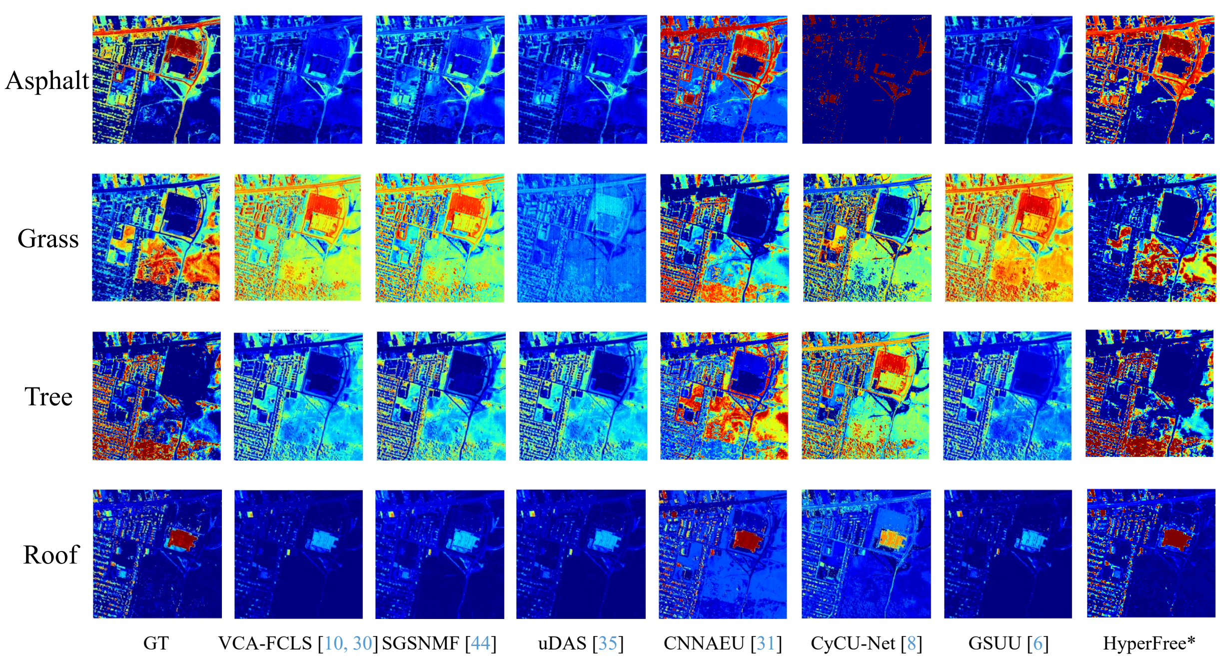

Figure 15. Qualitative comparison results on Urban dataset of HU task, where HyperFree* represents the tuning version.

Table 11. Quantitative comparison results on HOT task in tuning manner, where HyperFree* represents the tuning version and blue numbers indicate the metric ranking.

Data	Metrics	BAENet [23]	MHT [48]	SiamHYPER [25]	SEE-Net [24]	SiamBAG [21]	TSCFW [11]	HyperFree*
HOTC 2023 [1]	AUC	0.496	0.465	0.564	0.499	0.508	0.476	0.576(1st)
	DP	0.757	0.733	0.778	0.737	0.736	0.708	0.796(1st)
	FPS	0.8	0.5	29.8	16.8	14.1	4.1	16.4(3rd)

Name: VIS_Coke **Attributes**: BC, IPR, OPR, FM, SV **Name**: NIR_Car59 **Attributes**: OCC, SV, FM **Name**: RedNIR_Dice2 **Attributes**: LR, BC, OCC

Figure 16. Qualitative comparison results on HOCT 2023 dataset of HOT task, where HyperFree* represents the tuning version.

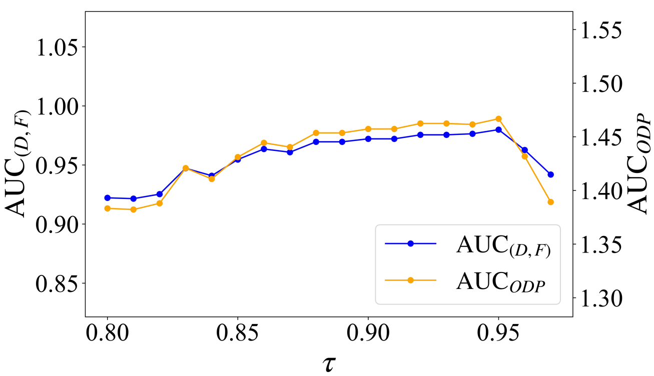

(a) HTD on Cri Dataset

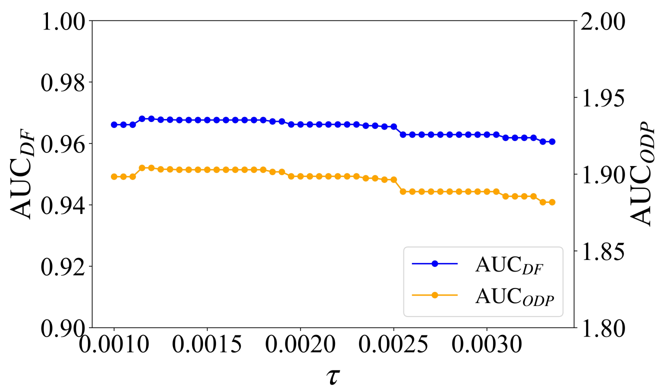

(b) HAD on Beanch Dataset

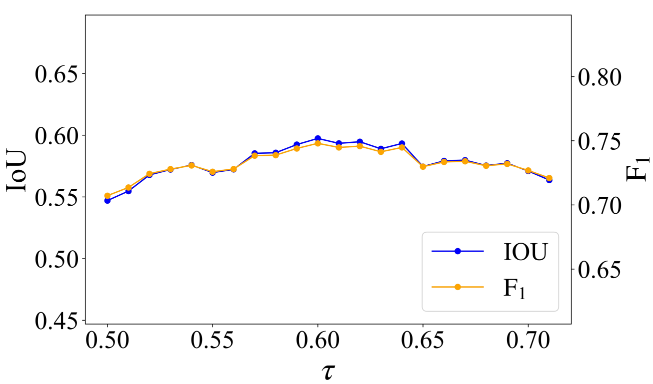

(c) HCD on Hermiston Dataset

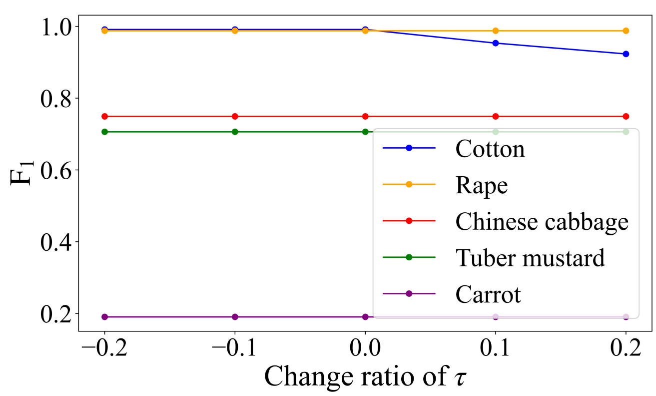

(d) HOCC on HongHu Dataset

Figure 17. Sensitivity analysis of the hyperparameter τ on the model performance.

References

[1] https://www.hsitracking.com/. 1, 3

[2] http://xudongkang.weebly.com/data-sets.html. 1, 3

[3] https://engineering.purdue.edu/~biehl/MultiSpec/hyperspectral.html. 1, 3

[4] Chein-I Chang. Constrained energy minimization (cem) for hyperspectral target detection: Theory and generalizations. *IEEE Transactions on Geoscience and Remote Sensing*, 2024. 3

[5] Hao Chen, Zipeng Qi, and Zhenwei Shi. Remote sensing image change detection with transformers. *IEEE Transactions on Geoscience and Remote Sensing*, 60:1–14, 2021. 1, 3

[6] Chunyang Cui, Xinyu Wang, Shaoyu Wang, Liangpei Zhang, and Yanfei Zhong. Unrolling nonnegative matrix factorization with group sparsity for blind hyperspectral unmixing. *IEEE Transactions on Geoscience and Remote Sensing*, 2023. 3

[7] Rodrigo Caye Daudt, Bertr Le Saux, and Alexandre Boulch. Fully convolutional siamese networks for change detection. In *2018 25th IEEE international conference on image processing (ICIP)*, pages 4063–4067. IEEE, 2018. 3

[8] Lianru Gao, Zhu Han, Danfeng Hong, Bing Zhang, and Jocelyn Chanussot. Cycu-net: Cycle-consistency unmixing network by learning cascaded autoencoders. *IEEE Transactions on Geoscience and Remote Sensing*, 60:1–14, 2021. 3

[9] Wei He, Quanming Yao, Chao Li, Naoto Yokoya, and Qibin Zhao. Non-local meets global: An integrated paradigm for hyperspectral denoising. In *Proceedings of the IEEE/CVF Conference on Computer Vision and Pattern Recognition*, pages 6868–6877, 2019. 3

[10] Daniel C Heinz et al. Fully constrained least squares linear spectral mixture analysis method for material quantification in hyperspectral imagery. *IEEE transactions on geoscience and remote sensing*, 39(3):529–545, 2001. 3

[11] Zengfu Hou, Wei Li, Jun Zhou, and Ran Tao. Spatial–spectral weighted and regularized tensor sparse correlation filter for object tracking in hyperspectral videos. *IEEE Transactions on Geoscience and Remote Sensing*, 60:1–12, 2022. 3

[12] Meiqi Hu, Chen Wu, and Liangpei Zhang. Globalmind: Global multi-head interactive self-attention network for hyperspectral change detection. *ISPRS Journal of Photogrammetry and Remote Sensing*, 211:465–483, 2024. 1, 3

[13] Wenpeng Hu, Ran Le, Bing Liu, Feng Ji, Jinwen Ma, Dongyan Zhao, and Rui Yan. Predictive adversarial learning from positive and unlabeled data. In *Proceedings of the AAAI conference on artificial intelligence*, pages 7806–7814, 2021. 2

[14] Jinyue Jiao, Zhiqiang Gong, and Ping Zhong. Triplet spectral-wise transformer network for hyperspectral target detection. *IEEE Transactions on Geoscience and Remote Sensing*, 2023. 1, 3

[15] Linda S Kalman and Edward M Bassett III. Classification and material identification in an urban environment using hydice hyperspectral data. In *Imaging Spectrometry III*, pages 57–68. SPIE, 1997. 1, 3

[16] Ryuichi Kiryo, Gang Niu, Marthinus C Du Plessis, and Masashi Sugiyama. Positive-unlabeled learning with non-negative risk estimator. *Advances in neural information processing systems*, 30, 2017. 2

[17] Shawn Kraut, Louis L Scharf, and L Todd McWhorter. Adaptive subspace detectors. *IEEE Transactions on signal processing*, 49(1):1–16, 2001. 3

[18] Jingtao Li, Xinyu Wang, Shaoyu Wang, Hengwei Zhao, and Yanfei Zhong. One step detection paradigm for hyperspectral anomaly detection via spectral deviation relationship learning. *IEEE Transactions on Geoscience and Remote Sensing*, 2024. 1, 3

[19] Miaoyu Li, Ying Fu, and Yulun Zhang. Spatial-spectral transformer for hyperspectral image denoising. In *Proceedings of the AAAI Conference on Artificial Intelligence*, pages 1368–1376, 2023. 3

[20] Wei Li and Qian Du. Collaborative representation for hyperspectral anomaly detection. *IEEE Transactions on geoscience and remote sensing*, 53(3):1463–1474, 2014. 3

[21] Wei Li, Zengfu Hou, Jun Zhou, and Ran Tao. Siambag: Band attention grouping-based siamese object tracking network for hyperspectral videos. *IEEE Transactions on Geoscience and Remote Sensing*, 61:1–12, 2023. 3

[22] Yapeng Li, Yong Luo, Lefei Zhang, Zengmao Wang, and Bo Du. Mambahsi: Spatial–spectral mamba for hyperspectral image classification. *IEEE Transactions on Geoscience and Remote Sensing*, 62:1–16, 2024. 1, 2

[23] Zhuanfeng Li, Fengchao Xiong, Jun Zhou, Jing Wang, Jianfeng Lu, and Yuntao Qian. Bae-net: A band attention aware ensemble network for hyperspectral object tracking. In *2020 IEEE international Conference on image processing (ICIP)*, pages 2106–2110. IEEE, 2020. 3

[24] Zhuanfeng Li, Fengchao Xiong, Jun Zhou, Jianfeng Lu, and Yuntao Qian. Learning a deep ensemble network with band importance for hyperspectral object tracking. *IEEE Transactions on Image Processing*, 32:2901–2914, 2023. 3

[25] Zhenqi Liu, Xinyu Wang, Yanfei Zhong, Meng Shu, and Chen Sun. Siamhyper: Learning a hyperspectral object tracker from an rgb-based tracker. *IEEE Transactions on Image Processing*, 31:7116–7129, 2022. 3

[26] Dimitris Manolakis and Gary Shaw. Detection algorithms for hyperspectral imaging applications. *IEEE signal processing magazine*, 19(1):29–43, 2002. 3

[27] Dimitris Manolakis, Eric Truslow, Michael Pieper, Thomas Cooley, and Michael Brueggeman. Detection algorithms in hyperspectral imaging systems: An overview of practical algorithms. *IEEE Signal Processing Magazine*, 31(1):24–33, 2013. 3

[28] Farid Melgani and Lorenzo Bruzzone. Classification of hyperspectral remote sensing images with support vector machines. *IEEE Transactions on geoscience and remote sensing*, 42(8):1778–1790, 2004. 2

[29] Yu-Chun Miao, Xi-Le Zhao, Xiao Fu, Jian-Li Wang, and Yu-Bang Zheng. Hyperspectral denoising using unsupervised disentangled spatiospectral deep priors. *IEEE Trans. Geosci. Remote. Sens.*, 60:1–16, 2022. 3

[30] José MP Nascimento and José MB Dias. Vertex component analysis: A fast algorithm to unmix hyperspectral data. *IEEE*

transactions on Geoscience and Remote Sensing, 43(4):898–910, 2005. 3

[31] Burkni Palsson, Magnus O Ulfarsson, and Johannes R Sveinsson. Convolutional autoencoder for spectral–spatial hyperspectral unmixing. *IEEE Transactions on Geoscience and Remote Sensing*, 59(1):535–549, 2020. 3

[32] Jiangjun Peng, Qi Xie, Qian Zhao, Yao Wang, Leung Yee, and Deyu Meng. Enhanced 3dtv regularization and its applications on hsi denoising and compressed sensing. *IEEE Transactions on Image Processing*, 29:7889–7903, 2020. 3

[33] Rami Piiroinen, Fabian Ewald Fassnacht, Janne Heiskanen, Eduardo Maeda, Benjamin Mack, and Petri Pellikka. Invasive tree species detection in the eastern arc mountains biodiversity hotspot using one class classification. *Remote sensing of environment*, 218:119–131, 2018. 2

[34] Jiahui Qu, Shaoxiong Hou, Wenqian Dong, Yunsong Li, and Weiying Xie. A multilevel encoder–decoder attention network for change detection in hyperspectral images. *IEEE Transactions on Geoscience and Remote Sensing*, 60:1–13, 2021. 3

[35] Ying Qu and Hairong Qi. udas: An untied denoising autoencoder with sparsity for spectral unmixing. *IEEE Transactions on Geoscience and Remote Sensing*, 57(3):1698–1712, 2018. 3

[36] Ying Qu, Wei Wang, Rui Guo, Bulent Ayhan, Chiman Kwan, Steven Vance, and Hairong Qi. Hyperspectral anomaly detection through spectral unmixing and dictionary-based low-rank decomposition. *IEEE Transactions on Geoscience and Remote Sensing*, 56(8):4391–4405, 2018. 3

[37] Irving S Reed and Xiaoli Yu. Adaptive multiple-band cfar detection of an optical pattern with unknown spectral distribution. *IEEE transactions on acoustics, speech, and signal processing*, 38(10):1760–1770, 1990. 3

[38] Swalpa Kumar Roy, Gopal Krishna, Shiv Ram Dubey, and Bidyut B Chaudhuri. Hybridsn: Exploring 3-d–2-d cnn feature hierarchy for hyperspectral image classification. *IEEE Geoscience and Remote Sensing Letters*, 17(2):277–281, 2019. 2

[39] Bernhard Schölkopf, Robert C Williamson, Alex Smola, John Shawe-Taylor, and John Platt. Support vector method for novelty detection. *Advances in neural information processing systems*, 12, 1999. 2

[40] Dunbin Shen, Xiaorui Ma, Wenfeng Kong, Jianjun Liu, Jie Wang, and Hongyu Wang. Hyperspectral target detection based on interpretable representation network. *IEEE Transactions on Geoscience and Remote Sensing*, 2023. 1, 3

[41] Le Sun, Guangrui Zhao, Yuhui Zheng, and Zebin Wu. Spectral–spatial feature tokenization transformer for hyperspectral image classification. *IEEE Transactions on Geoscience and Remote Sensing*, 60:1–14, 2022. 1, 2

[42] Di Wang, Bo Du, and Liangpei Zhang. Fully contextual network for hyperspectral scene parsing. *IEEE Transactions on Geoscience and Remote Sensing*, 60:1–16, 2021. 2

[43] Shaoyu Wang, Xinyu Wang, Liangpei Zhang, and Yanfei Zhong. Auto-ad: Autonomous hyperspectral anomaly detection network based on fully convolutional autoencoder. *IEEE Transactions on Geoscience and Remote Sensing*, 60:1–14, 2021. 1, 3

[44] Xinyu Wang, Yanfei Zhong, Liangpei Zhang, and Yanyan Xu. Spatial group sparsity regularized nonnegative matrix factorization for hyperspectral unmixing. *IEEE Transactions on Geoscience and Remote Sensing*, 55(11):6287–6304, 2017. 3

[45] Yanheng Wang, Danfeng Hong, Jianjun Sha, Lianru Gao, Lian Liu, Yonggang Zhang, and Xianhui Rong. Spectral–spatial–temporal transformers for hyperspectral image change detection. *IEEE Transactions on Geoscience and Remote Sensing*, 60:1–14, 2022. 1, 3

[46] Kaixuan Wei, Ying Fu, and Hua Huang. 3-d quasi-recurrent neural network for hyperspectral image denoising. *IEEE transactions on neural networks and learning systems*, 32 (1):363–375, 2020. 3

[47] Fengchao Xiong, Jun Zhou, and Yuntao Qian. Hyperspectral restoration via l_0 gradient regularized low-rank tensor factorization. *IEEE Transactions on Geoscience and Remote Sensing*, 57(12):10410–10425, 2019. 3

[48] Fengchao Xiong, Jun Zhou, and Yuntao Qian. Material based object tracking in hyperspectral videos. *IEEE Transactions on Image Processing*, 29:3719–3733, 2020. 3

[49] Yang Xu, Zebin Wu, Jun Li, Antonio Plaza, and Zhihui Wei. Anomaly detection in hyperspectral images based on low-rank and sparse representation. *IEEE Transactions on Geoscience and Remote Sensing*, 54(4):1990–2000, 2015. 3

[50] CEN Yi, Lifu Zhang, Xia Zhang, WANG Yueming, QI Wenchao, TANG Senlin, and Peng Zhang. Aerial hyperspectral remote sensing classification dataset of xiongan new area (matiwan village). *National Remote Sensing Bulletin*, 24 (11):1299–1306, 2020. 1, 2

[51] Yuxiang Zhang, Bo Du, Liangpei Zhang, and Shugen Wang. A low-rank and sparse matrix decomposition-based mahalanobis distance method for hyperspectral anomaly detection. *IEEE Transactions on Geoscience and Remote Sensing*, 54(3):1376–1389, 2015. 1, 3

[52] Hengwei Zhao, Xinyu Wang, Jingtao Li, and Yanfei Zhong. Class prior-free positive-unlabeled learning with taylor variational loss for hyperspectral remote sensing imagery. In *Proceedings of the IEEE/CVF International Conference on Computer Vision*, pages 16827–16836, 2023. 1, 2

[53] Hengwei Zhao, Yanfei Zhong, Xinyu Wang, and Hong Shu. One-class risk estimation for one-class hyperspectral image classification. *IEEE Transactions on Geoscience and Remote Sensing*, 2023. 1, 2

[54] Zhuo Zheng, Yanfei Zhong, Ailong Ma, and Liangpei Zhang. Fpga: Fast patch-free global learning framework for fully end-to-end hyperspectral image classification. *IEEE Transactions on Geoscience and Remote Sensing*, 58(8):5612–5626, 2020. 2

[55] Yanfei Zhong, Xin Hu, Chang Luo, Xinyu Wang, Ji Zhao, and Liangpei Zhang. Whu-hi: Uav-borne hyperspectral with high spatial resolution (h2) benchmark datasets and classifier for precise crop identification based on deep convolutional neural network with crf. *Remote Sensing of Environment*, 250:112012, 2020. 1, 2